analytical chemistry

pubs.acs.org/ac Article

Paper-Based Bipolar Electrode Electrochemiluminescence Platform for Detection of Multiple miRNAs

Fangfang Wang,[⊥] Yunqing Liu,[⊥] Cuiping Fu, Na Li, Miao Du,* Lina Zhang,* Shenguang Ge,* and Jinghua Yu

Cite This: *Anal. Chem.* 2021, 93, 1702−1708 Read Online

ACCESS | Metrics & More | Article Recommendations | Supporting Information

ABSTRACT: This paper introduces a novel potential-resolved paper-based biosensor for simultaneous detection of multiple microRNAs (miRNAs) (taking miRNA-155 and miRNA-126 as examples) based on the bipolar electrode (BPE) electrochemiluminescence (ECL) strategy. The proposed multiple-channel paper-based sensing microfluidic platform was prepared by wax-printing technology, screen-printing method, and in situ Au nanoparticles (AuNPs) growth to form hydrophilic areas, hydrophobic boundaries, waterproof electronic bridge, driving electrode regions, and parallel bipolar electrode regions. CdTe quantum dots (QDs)-H2 and Au@g-C_3N_4 nanosheets (NSs)-DNA1 were used as dual electrochemiluminescence signal probes, and carboxylated Fe_3O_4 magnetic nanoparticles existed as carriers. CdTe QDs-H2/$S_2O_8^{2-}$ and Au@g-C_3N_4 NSs-DNA1/$S_2O_8^{2-}$ could exhibit two strong and stable ECL emissions at a drive voltage of 9 and 12 V, respectively, which can be used as effective potential-resolved signal tags. In addition, the proposed three-dimensional (3D) DNA nanomachine model and the target miRNA cycle strategy were used to achieve double amplification of electrochemiluminescence intensity. More importantly, the combination of the bipolar electrode system and the potential-resolved multitarget electrochemiluminescence method can greatly reduce the spatial interference between substances. The prepared ECL biosensor showed a favorable linear response for the detection of miRNA-155 and miRNA-126 with relatively low detection limits of 5.7 and 4.2 fM, respectively. With excellent sensitivity, the strategy may provide an efficient method for clinical application, especially in detection of trace multiple targets.

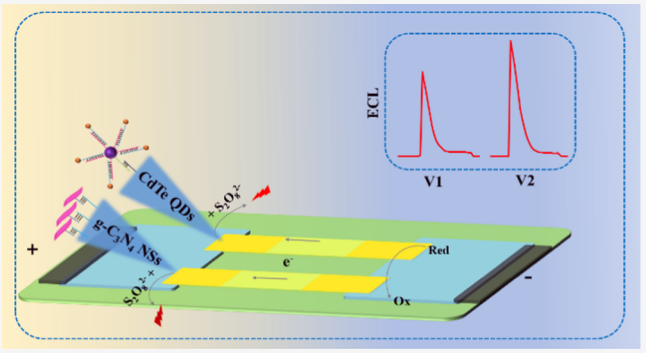

INTRODUCTION

MicroRNAs (miRNAs) as drug discovery targets or important clinical biomarkers for cancer and other diseases (diabetes, leukemia, cardiovascular disease, etc.) have attracted wide attention for their accurate and sensitive detection.[1−3] Nowadays, there are many popular strategy methods for detecting crucial biomarkers, including fluorescence[4] (FL), chemiluminescence[5] (CL), electrochemistry,[6] electrochemiluminescence (ECL),[7] colorimetry,[8] and so on. Among them, electrochemiluminescence has been considered as one of the most popular detection methods, which combines the advantages of both electrochemistry and photochemistry. In recent years, a variety of ECL biosensors[9−11] have been manufactured and showed a broad application prospect because of the fast response time, high sensitivity, and low cost. Due to the low concentration of miRNA in biological samples, it is crucial to improve the detection sensitivity. The traditional three-electrode detection method[12−14] has certain spatial interference problems (such as interference between electrode contacts, interference of electrolyte solution on electron transfer, etc.). On the one hand, two kinds of luminescent probes were modified on the BPE cathode, which avoids the direct contact between photoactive molecules and the complex reaction system and increases the information obtained by a single detection. On the other hand, the physical spacing between the cathode and anode and the structure of the chip enable high-sensitivity ECL detection of miRNAs.

The traditional BPE-ECL detection system usually uses complex and relatively expensive microfluidic technology to integrate the detection unit into the microchip laboratory equipment,[15,16] which requires expensive equipment or skilled personnel; thus, it limits the effectiveness for immediate medical diagnostics. Nevertheless, these problems can be solved by microfluidic paper-based analysis equipment,[17,18] which has attracted increasing attention in the field of

Received: October 13, 2020
Accepted: December 14, 2020
Published: December 28, 2020

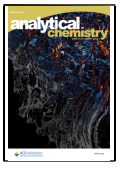

https://dx.doi.org/10.1021/acs.analchem.0c04307
Anal. Chem. 2021, 93, 1702−1708

bioanalysis and detection because of its affordable price, easy folding, and good biocompatibility.[19−21] Paper-based microfluidic BPE-ECL detection chips can be constructed by inkjet-printing, wax-printing, or screen-printing technology. More importantly, compared with traditional detection and analysis methods, through the pattern processing and reasonable partition of paper scraps, it is possible to detect two components or even multiple components at the same time on one detection platform.[22] Therefore, we developed a paper-based BPE-ECL sensing platform to realize the qualitative and quantitative detection of multiple miRNAs, such as miRNA-155 and miRNA-126.

Owing to the diversity, predictability, and fine specificity of DNA hybridization, DNA-based nanomachines have been successfully constructed, such as DNA walker, DNA motor, and DNA tweezers.[23,24] These DNA machines can be activated by external inputs, usually accompanied by conformational changes in the functional DNA under molecular interactions. However, most DNA nanomachines operate on one-dimensional or two-dimensional trajectories, which lead to the limitations of low maneuverability and cargo payload.[25,26] Meanwhile, a three-dimensional (3D) DNA nanomachine has been considered as a promising solution because of its inherent advantages, including high cargo loading capacity, accelerating target recovery dynamics, and so on.[27,28] For example, Zheng et al.[29] introduced a new 3D DNA nanomachine that was driven by proteins or nucleic acids; Li et al.[30] reported a DNA nanomachine that was made of DNA-functionalized AuNPs and enabled DNA rovers to move along 3D DNA-AuNP orbits and performed the task of releasing payloads. More importantly, the 3D DNA nanomachine running on three-dimensional nanomaterials exhibits a satisfactory signal amplification effect for nucleic acid or protein detection because of its improved mobility, high DNA loading efficiency, and increased walking steps.[31−33] Besides, as a 3D DNA nanomachine signal probe carrier, Fe_3O_4 magnetic nanoparticles have been adopted by us because of their large surface area, fast separation speed, high DNA load density, and so on.[34] Based on the advantages of 3D DNA nanomachines, nanomachines were constructed to capture different electrochemiluminescence signal probes to detect a variety of miRNAs.

The key to successfully preparing a potential-resolved ECL-BPE biosensor is to prepare electrochemiluminescence probes with distinguishable potential excitation light signal.[35−37] In this study, CdTe QDs[12,37] and g-C_3N_4 NSs[38,39] were selected as potential-resolved ECL probes to emit electrochemiluminescence signals in the presence of the co-reactant $K_2S_2O_8$ at potentials of 9 and 12 V, respectively. Additionally, the 3D DNA nanomachine was used to circulate the target and form signal probes, which can further enhance the electrochemiluminescence signal and improve the detection sensitivity.[40] Then, a patterned bipolar sensor paper chip with obvious partitions was constructed, and two electrochemiluminescence intensities were observed on the cathode by changing the driving voltage of the BPE, indicating that potential-resolving electrochemiluminescence devices can indeed be developed with parallel BPE. The proposed method is suitable for simultaneous detection of dual-target miRNAs and is of great value in improving the accuracy and reliability of early diagnosis.

EXPERIMENTAL SECTION

Materials and Apparatus. The materials and apparatus are described in the Supporting Information S1.

Synthesis of the 3D DNA Nanomachine Signal Probe Fe_3O_4-S2-H1-H2-CdTe QDs. First, different concentrations of miRNA-155 and CdTe QDs-H2 (see the Supporting Information S3.1) with a total volume of 10 μL were added to 20 μL of Fe_3O_4-S2-H1 magnetic nanomaterial solution (see the Supporting Information S3.2). Then, a 3D-DNA nanomechanical signal probe (Fe_3O_4-S2-H1-H2-CdTe QDs) was formed after incubation for 2 h. Finally, the obtained Fe_3O_4-S2-H1-H2-CdTe QDs signal probe was dispersed in 20 μL of PBS (pH 7.4) for further use after the unreacted reagent was removed by magnetic separation.

Synthesis of the Signal Probe ST-Au@g-C_3N_4 NSs. To begin with, h1 (10 μL, 0.5 μM), 60 μL of Au@g-C_3N_4 NSs-DNA1 solution (see the Supporting Information S3.3), and the mixture of EDC (20 μL, 0.2 M) and NHS (20 μL, 0.05 M) were added into the purchased carboxylated Fe_3O_4 magnetic nanoparticles at 4 °C and allowed to stand for 5 h to form the 3D DNA nanomachine. The above solution was magnetically separated and washed to remove the unbounded reactants. Subsequently, the mixture, with a total volume of 10 μL, including different concentrations of miRNA-126 and h2 was mixed with the prepared 3D DNA nanomachine solution (10 μL) and shaken at room temperature for 2 h. When the miRNA-126 was introduced into the system, it further opened hairpin h1 to hybridize with hairpin h2 immediately and the unhybridized portion of h2 (walker probe) was combined with the DNA1-Au@g-C_3N_4 NSs. After completion of the above process, the specific enzyme recognition site was produced. In the presence of Nt.BbvCI, the walker probe was sheared, released, and walked along the 3D track, producing a large number of DNA1-Au@g-C_3N_4 NS single-stranded fragments, which were used as the simulated target product (ST-Au@g-C_3N_4 NSs). Finally, the supernatant obtained by magnetic separation technology, namely, ST-Au@g-C_3N_4 NS solution, was stored at 4 °C for further testing.

Fabrication of the Potential-Resolved Dual-Target BPE-ECL Biosensor. First, the pattern of the paper chip was designed with the aid of Adobe Illustrator (AI) software (shown in Figure S1). The No. 1 paper was cut into a size of A4 paper, and physical drawings were printed by a wax-printing technology according to the design drawings. Then, the printed paper chip was baked in an oven (130 °C, 60 s), and the same size (12 × 12 mm^2) blank reaction zone (hydrophilic region), wax infiltration region (hydrophobic zone), two bipolar electrode regions (2 × 5 × 15 mm^3), and waterproof salt bridge region (2 × 5 × 6 mm^3) were formed. In addition, the drive electrode was printed via screen printing to connect the direct current (DC) power supply. Then, referring to the previous work experience,[3] AuNPs were grown in situ on the surface of the paper fiber in the bipolar electrode region to form a BPE with excellent conductivity. Finally, the prepared Au-BPE surface was washed and dried to remove the floating color.

First, S1 (10 μL, 2.5 μM) and DNA2 (10 μL, 2.5 μM) were dripped on the AuNP-modified electrode surfaces a and b and incubated at 4 °C for 16 h. Then, the electrode surfaces were blocked with MCH and MEA for 2 h after washing thoroughly with PBS (pH 7.4), respectively. Afterward, the prepared signal probes Fe_3O_4-S2-H1-H2-CdTe QDs (10 μL) and ST-Au@g-

https://dx.doi.org/10.1021/acs.analchem.0c04307
Anal. Chem. 2021, 93, 1702−1708

Scheme 1. Preparation of the Paper-Based Potential-Resolved BPE-ECL Biosensor for the Detection of miRNA-155 and miRNA-126[a]

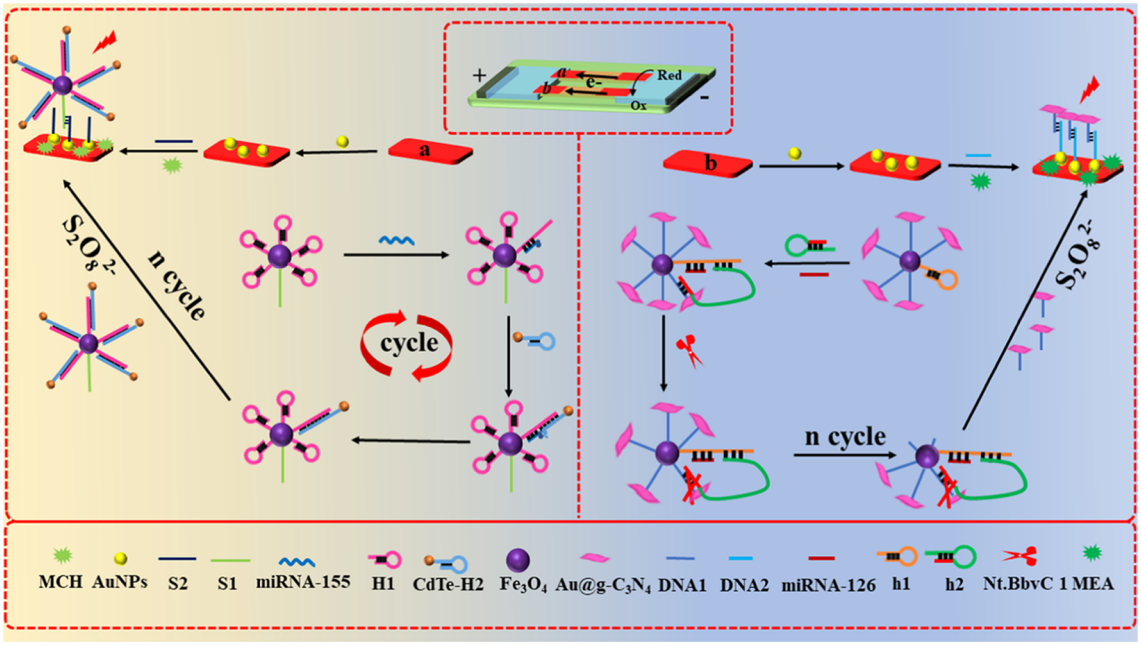

[a]The step-by-step formation process of the 3D-DNA nanomechanical signal probe (Fe_3O_4-S2-H1-H2-CdTe QDs) and the cyclic process of the target miRNA-155 occur at the cathode of the bipolar electrode a; miRNA-126-driven 3D nanomachine cycle amplification process and ST-Au@g-C_3N_4 NSs release process occur at the cathode of the bipolar electrode b.

C_3N_4 NSs (10 μL) were dropped onto the electrode surfaces modified with S1-Au-BPE and DNA2-Au-BPE and incubated at 37 °C for 2 h. Finally, the surfaces of the parallel Au-BPE electrodes were washed with PBS to remove probes that were not bound to the site. The paper-based chip was folded in half along the center line so that the hydrophilic areas are completely in contact with the two BPEs on the other side. The DC driving voltages of 9 and 12 V were applied and the PMT high voltage was set to be 800 V for the next step of target detection.

RESULTS AND DISCUSSION

Principle of the Paper-Based Dual-Channel BPE-ECL Biosensor. Scheme 1 shows the construction of parallel bipolar electrode devices and the principle of electrochemiluminescence strategy for the detection of multiple targets (miRNA-155 and miRNA-126 are selected as examples). First, for the manufacture of the bipolar electrode device, the paper-chip model of the parallel bipolar electrode was established on the basis of previous research.[3,17] In short, the prototype of the paper chip was formed through AI software design, screen-printing technology, and wax-printing technology. Then, the paper was baked in an oven for 60 s (130 °C) to soak the wax through the paper fiber to form hydrophilic regions, hydrophobic boundary, and parallel bipolar electrode regions (AuNPs grown in situ), driving voltage regions and hydrophobic salt bridge region (a picture of a paper-based closed bipolar electrode is shown in the Supporting Information, Figure S2). Second, in the process of detecting multiple targets, due to the connection between the cathode and the anode, the electron transfer process in each bipolar electrode was electrically coupled with the ECL reaction of each light-emitting probe. Therefore, the electron transfer process driven by the voltage occurred between the two poles of the BPE. In detail, the DC power supply was connected to the parallel bipolar electrode sensing platform, and the most suitable driving voltages (as shown in the Supporting Information, Figure S4) for the two light-emitting probes (CdTe QDs and g-C_3N_4 NSs) with their co-reactants were executed. The paper chip was folded so that the parallel BPE was in close contact with the two hydrophilic units. In the presence of CdTe QDs, by applying a driving voltage of 9 V to the co-reactant $K_2S_2O_8$ in the hydrophilic unit, which is in close contact with the cathode region of the parallel bipolar electrode, a process of excitation−radiative transition occurs, with the emission of light signal (the process of obtaining electrons). At the same time, when the driving voltage was applied, an oxidation reaction occurred at the anode when the bipolar electrode is in contact with the solution containing H_2O_2 (the mechanism of this process may be that H_2O_2 or H_2O was oxidized), so the entire bipolar electrode became the only electron transfer between the cathode and anode path. Similarly, changing the driving voltage to 12 V, in the process of detecting miRNA-126, the g-C_3N_4 NSs at the bipolar electrode cathode reacted with $K_2S_2O_8$ to emit light signals, and the anode unit underwent an oxidation reaction to form a cathode−anode electronic coupling. More importantly, when the two luminescence systems coexist in one sensing platform, the ECL signal was stronger than that when they existed alone.

In the process of introducing the target detection auxiliary luminous probe, the 3D nanomachine was used to construct a multitarget detection biosensor with further amplified signal. For example, in the process of detecting miRNA-155, hairpins DNA H1 and S1 combined with Fe_3O_4 magnetic nanoparticles to form a 3D DNA nanomachine through the interaction between amino and carboxyl groups in the solution. Upon addition of the target miRNA-155, the hairpin structure of H1 was opened and hybridized with the target to form the double-

https://dx.doi.org/10.1021/acs.analchem.0c04307
Anal. Chem. 2021, 93, 1702−1708

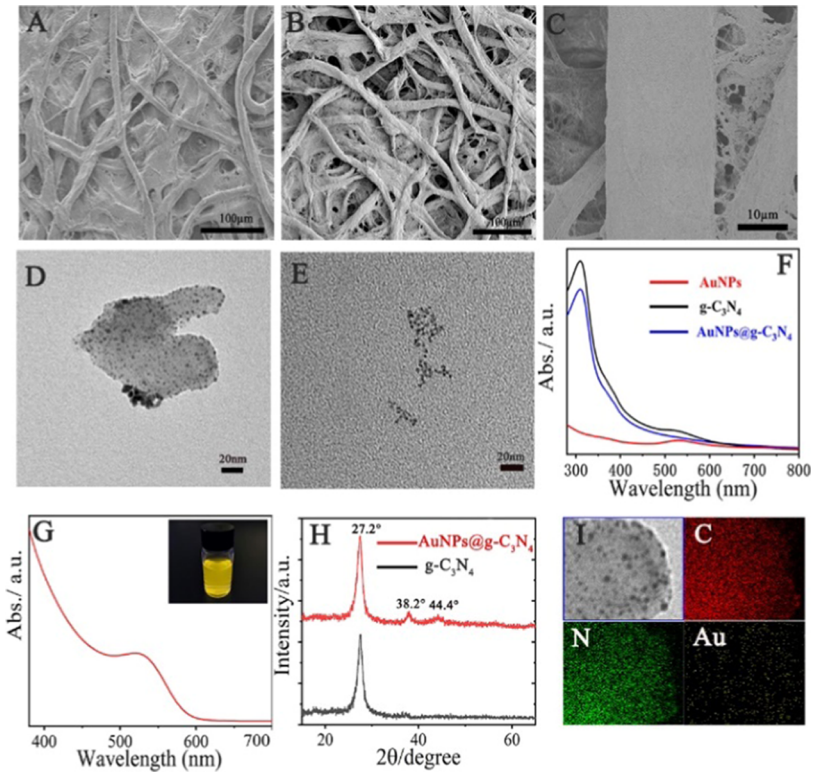

Figure 1. (A) SEM image of the bare paper. (B, C) SEM images of Au-BPE. TEM images of Au@g-C_3N_4 NSs (D) and CdTe QDs (E). (F) UV−vis absorption spectra of AuNPs, g-C_3N_4 NSs, and Au@g-C_3N_4 NSs. (G) UV−vis absorption spectra of CdTe QD solution. (H) XRD patterns of g-C_3N_4 NSs and Au@g-C_3N_4 NSs. (I) Elemental mapping images of Au@g-C_3N_4 NSs. Inset of (G) is the physical picture of CdTe QD solution.

stranded DNA hybrid H1-miRNA-155. Since the heterozygote structure of H1−H2 was more stable than the heterozygote of H1-miRNA-155, the target was replaced by H2-CdTe QDs and hybridized with H1 followed by the release of the target. After being released, the target molecules continued to participate in the next H2 cycle. After cycles, the 3D-DNA nanomechanical signal probe (Fe_3O_4-S2-H1-H2-CdTe QDs) was formed. Due to the complementary pairing of S1 and S2 bases, the Fe_3O_4-S2-H1-H2-CdTe QDs were successfully connected to the BPE cathode region. The reaction rate and the ECL intensity were greatly improved in the presence of the $K_2S_2O_8$ co-reactant and the 3D nanomachine. Therefore, using the nanomachine as an ECL signal probe and $K_2S_2O_8$ as a co-reactant to construct a biosensor can improve the detection sensitivity of the electrochemiluminescence biosensor. The paper-chip sensing detection platform with potential-resolved multitargets greatly improved the selectivity and sensitivity compared with the traditional sensing detection methods.

Characterization of Au-BPE, Au@g-C_3N_4 NSs, and CdTe QDs. The morphologies of involved nanomaterials were characterized by scanning electron microscopy (SEM) and transmission electron microscopy (TEM). Figure 1A shows the rough surface of the paper chip that consists of interlaced fibers, which greatly increases the specific surface area. The SEM image shown in Figure 1B displays the uniform distribution of AuNPs on each paper fiber, indicating the successful construction of Au-BPE (Figure 1C is a single paper fiber with AuNPs loaded in an enlarged version). For Au@g-C_3N_4 NSs (Figure 1D), the TEM image demonstrates that a large amount of AuNPs is uniformly anchored on the surface of g-C_3N_4 NSs (Figure S3 shows that g-C_3N_4 NSs have a two-dimensional flake structure), as g-C_3N_4 NSs carry positive charges while AuNPs carry negative charges. Figure 1E shows the TEM image of the prepared CdTe QDs, with an average size of 3−4 nm. At 520 nm of the ultraviolet−visible absorption spectrum (UV−vis) (Figure 1F), the absorption peak of Au@g-C_3N_4 NSs was observed, which can be indexed to the characteristic absorption peak of spherical AuNPs. UV−vis spectra (Figure 1G) are consistent with a previous study (illustration is a physical picture), with an absorption peak located at about 530 nm, which proves the successful synthesis of CdTe QDs.[41] The successful loading of AuNPs is further proved by XRD characterization (Figure 1H). The obtained g-C_3N_4 NSs exhibit a characteristic diffraction peak at 27.2° (black curve, Figure 1H), and the new diffraction peaks at 38.2 and 44.4° after the deposition of AuNPs are observed respectively (red curve, Figure 1H), indicating the deposition of AuNPs on g-C_3N_4 NSs. The elemental mapping of the Au@g-C_3N_4 NS composite sample in Figure 1I provides intuitive evidence that Au elements are homogeneously distributed on the surface of g-C_3N_4 NSs.

EIS Characterization of the Dual-Channel BPE-ECL Sensor. Electrochemical impedance spectroscopy (EIS) is an effective and simple technique to track the change in surface characteristics of the modified electrode during assembly and has been widely used in the characterization of biosensor fabrication process. Figure 2A shows the EIS curve of the gradual modification of BPE cathodes. As the modification processes of the double bipolar electrodes were similar, the step-by-step modification process when detecting miRNA-126 was taken as an example. It is observed that Au-BPE (Figure 2A, curve b) exhibits an EIS curve with a diameter smaller than that of bare paper BPE (Figure 2A, curve a) in the high frequency region, indicating a significant decrease of charge

https://dx.doi.org/10.1021/acs.analchem.0c04307
Anal. Chem. 2021, 93, 1702−1708

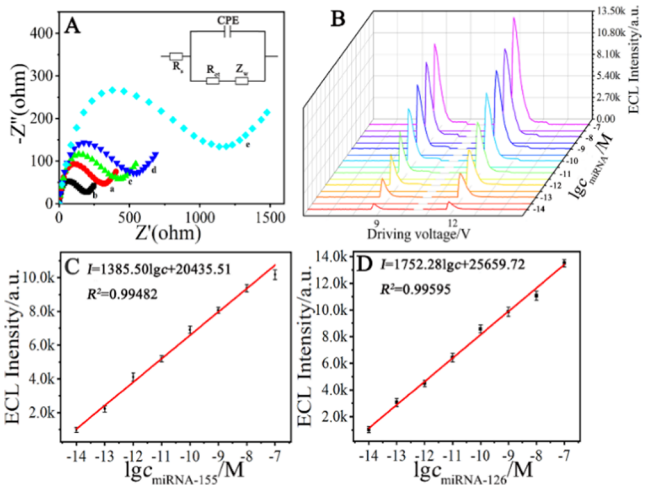

Figure 2. (A) EIS curves of electrodes with different modifications in PBS (0.1 M, pH 7.4) including 5.0 mM $[Fe(CN)_6]^{3-/4-}$ (an equimolar mixture of ferrocyanide and ferricyanide), (a) bare BPE, (b) Au-BPE, (c) DNA2/Au-BPE, (d) MEA/DNA2/Au-BPE, and (e) ST-Au@g-C_3N_4 NSs MEA/DNA2/Au-BPE. (B) ECL responses of the proposed biosensor in different concentrations of miRNA-155 (9 V) and miRNA-126 (12 V) in PBS (0.1 M, pH 7.4) containing 50 mM $S_2O_8^{2-}$. Calibration curves for (C) miRNA-155 and (D) miRNA-126 determination.

transfer resistance (R_{et}), which can be attributed to the conductivity increase caused by AuNP modification (Figure S5A). The continuously increasing R_{et} represented by the increasing diameters of the EIS curve further proves the successful modification of DNA2, MEA, and ST-Au@g-C_3N_4 NSs, respectively. The EIS curve of the miRNA-155-modified bipolar electrode is shown in the Supporting Information (Figure S5B). (Performance of miRNA detection contrasts with that of other works; see the Supporting Information, Table S2.)

Electrochemiluminescence Behaviors of Dual-Channel BPE-ECL Biosensor. Figure 3A–C shows the distribution of ECL intensity vs potential of a biosensor for detection of multiple targets of miRNA-155 alone, miRNA-126 alone, and both miRNA-155 and miRNA-126. The results show that the CdTe QDs and g-C_3N_4 NSs modified on the electrode produced two separate ECL emissions at 9 and 12 V, respectively. When the driving voltage was 9 V (as shown in Figure 3A), different concentrations of miRNA-155 and miRNA-126 were tested separately. The ECL intensity increased significantly with the increasing concentration of miRNA-155, but there was no obvious change with the concentration change of miRNA-126. Obviously, the ECL intensity during the detection of miRNA-155 was much greater than the intensity during the detection of miRNA-126. This was because only a large number of CdTe QDs/$K_2S_2O_8$ systems can be excited to emit light signals under 9 V voltage. Similarly, Figure 3A,B shows the case of independent detection of miRNA-155 and miRNA-126 when the driving voltage was 12 V. It can be seen that only miRNA-126 can be sensitively detected when the voltage was 12 V. The high ECL intensity during the detection of miRNA-126 was due to the fact that the g-C_3N_4 NSs/$K_2S_2O_8$ luminescence system was excited to generate a large number of light signals under the driving potential of 12 V. Finally, the effect of voltage on the ECL intensity of the parallel bipolar electrode sensor with different concentrations of dual targets coexisting was studied (Figure 3C). When the driving voltage was 9 V, the ECL intensity of the entire system was basically equivalent to the ECL intensity of miRNA-155 alone; there was even a slight increase, which may be attributed to the weak ECL intensity of the bipolar electrode on the side of miRNA-126 that was driven by the voltage, which caused the luminous intensity of the two to overlap. Similar to the above principle, when the driving voltage was 12 V, the ECL intensity of the entire system was basically equivalent to the ECL luminescence intensity of miRNA-126 alone with a slight increase. Therefore, the mutual interference between miRNA-155 and miRNA-126 on the same platform was negligible, and the specificity of the driving voltage for the detection of different targets was obvious. According to the changes of ECL intensity at two different potentials, miRNA-155 and miRNA-126 could be simultaneously detected on a microfluidic parallel bipolar electrode paper chip by changing the driving potential.

Detection of MiRNA-126 and MiRNA-155. For potential-resolved disposable paper-based BPE-ECL sensing platform, the signal was amplified through the target cycle process of DNA nanomachine formation in solution in this work. For the purpose of evaluating the sensitivity of the sensor platform, ECL detection was carried out for different concentrations of miRNA-126 and miRNA-155. As shown in Figure 2B, ECL intensity shows an increasing trend with the increase of the concentration of the two targets. There is a logarithmic relationship between the concentration of the targets and the electrochemiluminescence signal (see the Supporting Information, Figure S5C,D). The linear range of concentration was 1.0×10^{-14} to 1.0×10^{-7} M, and the linear regression equation of the detection for miRNA-155 (Figure 2C) was $I = 1385.50 \lg c + 20435.51$, with the regression

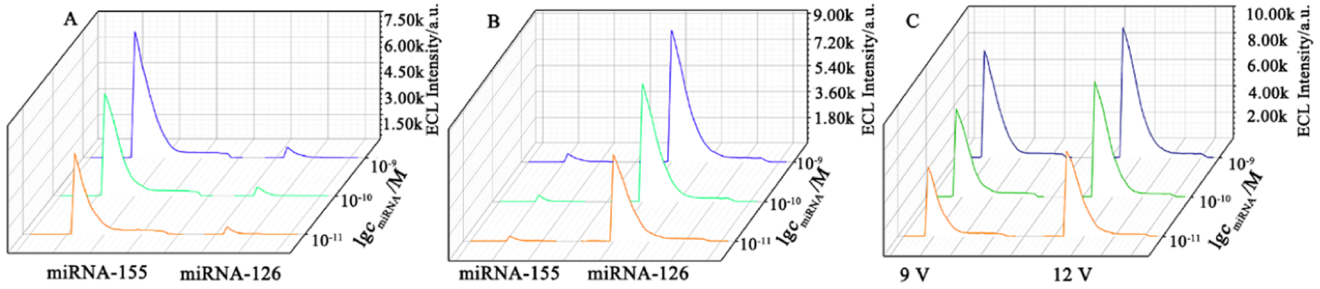

Figure 3. ECL intensity during separate detection of miRNA-155 and miRNA-126 at different concentrations. (A) Driving voltage: 9 V, (B) driving voltage: 12 V, and (C) ECL intensity of mixed solutions of different concentrations of miRNA-155 and miRNA-126 under different driving voltages.

https://dx.doi.org/10.1021/acs.analchem.0c04307
Anal. Chem. 2021, 93, 1702–1708

coefficient (R^2) as 0.99482; the linear regression equation of the detection for miRNA-126 (Figure 2D) was $I = 1752.28 \lg c + 25659.72$, with the regression coefficient (R^2) as 0.99595. The detection limits of miRNA-155 and miRNA-126 were calculated to be 5.7 and 4.2 fM (S/N = 3), respectively.

Specificity, Stability, and Reproducibility of the Proposed ECL Biosensor. The specificity of the designed biosensor was studied by introducing different interfering biomolecules. miRNA-126 (0.1 nM) was compared by adding other disturbances (blank, miRNA-141, miRNA-101, and miRNA-210 were included). It can be seen from Figure 4A

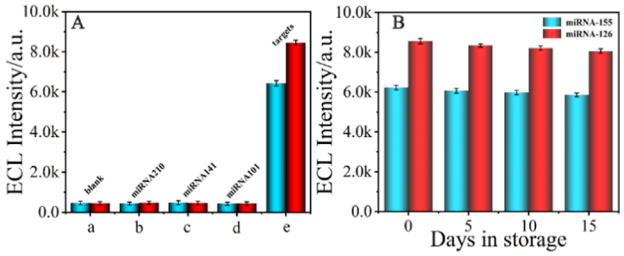

Figure 4. (A) Specificity of this proposed BPE-ECL biosensor for different interfering substances: (a) blank solution, (b) miRNA-210 (0.1 nM), (c) miRNA-141 (0.1 nM), (d) miRNA-101 (0.1 nM), (e) miRNA-155 (0.1 nM), and miRNA-126 (0.1 nM). (B) Stability of the proposed BPE-ECL biosensor.

that the modified biosensor has excellent specificity in the presence of other interferences. In the same way, the specificity of the miRNA-155 process was also detected, and good specificity was confirmed as shown in Figure 4A.

To study the long-term storage stability, the proposed parallel bipolar electrode electrochemiluminescence sensor was stored at 4 °C and the relative intensity of the ECL detected by the fixed concentration of miRNA-155 and miRNA-126 was regularly checked. When the biosensor was constructed freshly, the initial ECL intensities of miRNA-155 (0.1 nM) and miRNA-126 (0.1 nM) were obtained (Figure 4B). After storage for 5, 10, and 15 days, the ECL intensities of miRNA-155 were 97.4, 92.5, and 87.8% of the initial value, while those of miRNA-126 were 96.4, 93.5, and 86.3% of the initial value, respectively. Therefore, after several days of storage, the ECL intensity changes within an acceptable range, indicating that the biosensor has good storage stability.

Moreover, the reproducibility of the BPE-ECL biosensor was assessed by means of the differences (relative standard deviation (RSD)) of the intra-assays and inter-assays. Here, we used a standard solution including three different concentrations of miRNA-155 (10 pM, 10 nM, 0.1 μM) and miRNA-126 (10 pM, 10 nM, 0.1 μM) to evaluate the RSD ($n = 5$). The experimental data indicated that the RSD values of the intra-assay were 4.3, 5.2, and 3.9% at 10 pM, 10 nM, and 0.1 μM of miRNA-155 and the RSD values of the intra-assay were 4.9, 5.6, and 3.8% at 10 pM, 10 nM, and 0.1 μM of miRNA-126. However, the RSD values of the inter-assay using different batches of the BPE-ECL biosensor were 8.4, 7.2, and 9.0% at 10 pM, 10 nM, and 0.1 μM miRNA-155 and 8.7, 7.4, and 9.1% at 10 pM, 10 nM, and 0.1 μM miRNA-126, respectively. Thus, the reproducibility of the proposed biosensor was satisfactory.

CONCLUSIONS

In short, we have developed a potential-resolved BPE-ECL method for the detection of double targets miRNA-126 and miRNA-155. Through the pattern processing of the paper chip and the synergistic effect of closed Au-BPE and ECL, each area on the paper chip was relatively noncontact in space, which avoided the false-positive problem in the detection process. At the same time, the qualitative and quantitative detection of miRNA-126 and miRNA-155 was realized, which provided more useful information than the traditional one-time test and greatly improved the accuracy of detection. In addition, different driving voltages were applied to excite the reaction of the luminous substances and their co-reactants to achieve the detection of multiple targets on the same microfluidic paper-chip detection platform and increase the utilization rate of the paper chip. The advantages of paper chip include easy immobilization of biological macromolecules, including enzymes, proteins, DNA, and RNA, and its superiority of biocompatibility greatly broadens the variety of detected targets. Taken together, this work provided a novel method for constructing multitarget detection biosensors.

ASSOCIATED CONTENT

Supporting Information

The Supporting Information is available free of charge at https://pubs.acs.org/doi/10.1021/acs.analchem.0c04307.

Reagent and instrument; fabrication of the paper-based closed bipolar electrode device; synthesis of CdTe QDs-H2 and Fe_3O_4-H1-S2 magnetic nanomaterial; synthesis of Au@g-C_3N_4 NSs-DNA1; and electrochemical characterization of the potential-resolved bipolar electrode electrochemiluminescence biosensor (PDF)

AUTHOR INFORMATION

Corresponding Authors

Miao Du − *College of Chemistry, Chemical Engineering and Materials Science, Shandong Normal University, Jinan 250014, P. R. China*; Email: miaodu@sdnu.edu.cn

Lina Zhang − *Shandong Provincial Key Laboratory of Preparation and Measurement of Building Materials, School of Material Science and Engineering, University of Jinan, Jinan 250022, P. R. China*; Email: zhanglina818@126.com

Shenguang Ge − *Collaborative Innovation Center of Technology and Equipment for Biological Diagnosis and Therapy in Universities of Shandong, Institute for Advanced Interdisciplinary Research, University of Jinan, Jinan 250022, P. R. China*; orcid.org/0000-0002-0537-6491; Email: chm_gesg@163.com

Authors

Fangfang Wang − *Collaborative Innovation Center of Technology and Equipment for Biological Diagnosis and Therapy in Universities of Shandong, Institute for Advanced Interdisciplinary Research, University of Jinan, Jinan 250022, P. R. China*

Yunqing Liu − *Collaborative Innovation Center of Technology and Equipment for Biological Diagnosis and Therapy in Universities of Shandong, Institute for Advanced Interdisciplinary Research, University of Jinan, Jinan 250022, P. R. China*

Cuiping Fu − *Collaborative Innovation Center of Technology and Equipment for Biological Diagnosis and Therapy in Universities of Shandong, Institute for Advanced Interdisciplinary Research, University of Jinan, Jinan 250022, P. R. China*

https://dx.doi.org/10.1021/acs.analchem.0c04307
Anal. Chem. 2021, 93, 1702−1708

Na Li − *School of Chemistry and Chemical Engineering, University of Jinan, Jinan 250022, P. R. China*
Jinghua Yu − *School of Chemistry and Chemical Engineering, University of Jinan, Jinan 250022, P. R. China;* orcid.org/0000-0001-5043-0322

Complete contact information is available at: https://pubs.acs.org/10.1021/acs.analchem.0c04307

Author Contributions

[⊥]F.W. and Y.L. contributed equally to this work.

Notes

The authors declare no competing financial interest.

■ ACKNOWLEDGMENTS

This work was supported by the National Natural Science Foundation of China (21775055, 22074053, 21874055); Excellent Youth Innovation Team in Universities of Shandong (2019KJC016); The Project of "20 items of University" of Jinan (2018GXRC001); the Taishan Scholars program and Case-by-Case Project for Top Outstanding Talents of Jinan.

■ REFERENCES

(1) Liu, H.; Fan, J.; Liu, W.; Tong, C.; Xie, Z.; Deng, R.; Long, X. *Anal. Methods* **2018**, *10*, 5834−5841.
(2) Wang, H.; Jian, Y.; Kong, Q.; Liu, H.; Lan, F.; Liang, L.; Ge, S.; Yu, J. *Sens. Actuators, B* **2018**, *257*, 561−569.
(3) Wang, F.; Fu, C.; Huang, C.; Li, N.; Wang, Y.; Ge, S.; Yu, J. *Biosens. Bioelectron.* **2020**, *150*, No. 111917.
(4) Ye, Y.; Liu, K.; Geng, S.; Ji, J.; Sun, J.; Zhang, Y.; Pi, F.; Sun, X. *Sens. Actuators, B* **2019**, *301*, No. 126864.
(5) Sun, Y.; Lin, Y.; Sun, W.; Han, R.; Luo, C.; Wang, X.; Wei, Q. *Anal. Chim. Acta* **2019**, *1089*, 152−164.
(6) Rezaei, H.; Motovali-Bashi, M.; Radfar, S. *Anal. Chim. Acta* **2019**, *1092*, 66−74.
(7) Yang, X.; Yu, Y. Q.; Peng, L. Z.; Lei, Y. M.; Chai, Y. Q.; Yuan, R.; Zhuo, Y. *Anal. Chem.* **2018**, *90*, 3995−4002.
(8) Huang, L.; Zhang, X.; Zhang, Z. *Anal. Chim. Acta* **2018**, *1044*, 119−130.
(9) Hu, S.; Gao, J. *J. Phys. Chem. C* **2018**, *122*, 9054−9061.
(10) Liu, J. L.; Tang, Z. L.; Zhuo, Y.; Chai, Y. Q.; Yuan, R. *Anal. Chem.* **2017**, *89*, 9108−9115.
(11) Lei, Y. M.; Zhou, J.; Chai, Y. Q.; Zhuo, Y.; Yuan, R. *Anal. Chem.* **2018**, *90*, 12270−12277.
(12) Gao, X.; Fu, K.; Fu, L.; Wang, H.; Zhang, B.; Zou, G. *Biosens. Bioelectron.* **2020**, *150*, No. 111880.
(13) Ma, M. N.; Zhuo, Y.; Yuan, R.; Chai, Y. Q. *Anal. Chem.* **2015**, *87*, 11389−11397.
(14) Peng, H.; Huang, Z.; Wu, W.; Liu, M.; Huang, K.; Yang, Y.; Deng, H.; Xia, X.; Chen, W. *ACS Appl. Mater. Interfaces* **2019**, *11*, 24812−24819.
(15) Liu, H.; Zhou, X.; Liu, W.; Yang, X.; Xing, D. *Anal. Chem.* **2016**, *88*, 10191−10197.
(16) Shi, H. W.; Zhao, W.; Liu, Z.; Liu, X. C.; Xu, J. J.; Chen, H. Y. *Anal. Chem.* **2016**, *88*, 8795−8801.
(17) Ge, S.; Zhao, J.; Wang, S.; Lan, F.; Yan, M.; Yu, J. *Biosens. Bioelectron.* **2018**, *102*, 411−417.
(18) Feng, Q. M.; Pan, J. B.; Zhang, H. R.; Xu, J. J.; Chen, H. Y. *Chem. Commun.* **2014**, *50*, 10949−10951.
(19) Zheng, X.; Li, L.; Cui, K.; Zhang, Y.; Zhang, L.; Ge, S.; Yu, J. *ACS Appl. Mater. Interfaces* **2018**, *10*, 3333−3340.
(20) Ye, D.; Li, L.; Li, Z.; Zhang, Y.; Li, M.; Shi, J.; Wang, L.; Fan, C.; Yu, J.; Zuo, X. *Nano Lett.* **2019**, *19*, 369−374.
(21) Jiao, Y.; Du, C.; Zong, L.; Guo, X.; Han, Y.; Zhang, X.; Li, L.; Zhang, C.; Ju, Q.; Liu, J.; Yu, H.-D.; Huang, W. *Sens. Actuators, B* **2020**, *306*, No. 127239.
(22) Zhang, X.; Bao, N.; Luo, X.; Ding, S. N. *Biosens. Bioelectron.* **2018**, *114*, 44−51.
(23) Chen, Z.; Wang, C.; Hao, L.; Gao, R.; Li, F.; Liu, S. *Biosens. Bioelectron.* **2019**, *128*, 104−112.
(24) Feng, C.; Wang, Z.; Chen, T.; Chen, X.; Mao, D.; Zhao, J.; Li, G. *Anal. Chem.* **2018**, *90*, 2810−2815.
(25) Liu, J.-L.; Tang, Z.-L.; Zhang, J.-Q.; Chai, Y.-Q.; Zhuo, Y.; Yuan, R. *Anal. Chem.* **2018**, *90*, 5298−5305.
(26) Mason, S. D.; Tang, Y.; Li, Y.; Xie, X.; Li, F. *Trends Anal. Chem.* **2018**, *107*, 212−221.
(27) Jiang, X.; Wang, H.; Wang, H.; Zhuo, Y.; Yuan, R.; Chai, Y. *Anal. Chem.* **2017**, *89*, 4280−4286.
(28) Qing, M.; Xie, S.; Cai, W.; Tang, D.; Tang, Y.; Zhang, J.; Yuan, R. *Anal. Chem.* **2018**, *90*, 11439−11445.
(29) Zheng, J.; Ji, X.; Du, M.; Tian, S.; He, Z. *Nanoscale* **2018**, *10*, 17206−17211.
(30) Li, D.; Zhou, W.; Yuan, R.; Xiang, Y. *Anal. Chem.* **2017**, *89*, 9934−9940.
(31) Li, N.; Du, M.; Liu, Y.; Ji, X.; He, Z. *ACS Sens.* **2018**, *3*, 1283−1290.
(32) Li, Y.; Wang, G. A.; Mason, S. D.; Yang, X.; Yu, Z.; Tang, Y.; Li, F. *Chem. Sci.* **2018**, *9*, 6434−6439.
(33) Liu, J.; Cui, M.; Zhou, H.; Yang, W. *ACS Sens.* **2017**, *2*, 1847−1853.
(34) Tu, T. T.; Lei, Y. M.; Chai, Y. Q.; Zhuo, Y.; Yuan, R. *ACS Appl. Mater. Interfaces* **2020**, *12*, 3945−3952.
(35) Guo, Z.; Wu, L.; Hu, Y.; Wang, S.; Li, X. *Biosens. Bioelectron.* **2017**, *95*, 27−33.
(36) Han, F.; Jiang, H.; Fang, D.; Jiang, D. *Anal. Chem.* **2014**, *86*, 6896−6902.
(37) Lv, W.; Ye, H.; Yuan, Z.; Liu, X.; Chen, X.; Yang, W. *Trends Anal. Chem.* **2020**, *123*, No. 115767.
(38) Chen, L.; Zeng, X.; Si, P.; Chen, Y.; Chi, Y.; Kim, D. H.; Chen, G. *Anal. Chem.* **2014**, *86*, 4188−4195.
(39) Yin, X.; Liang, L.; Zhao, P.; Lan, F.; Zhang, L.; Ge, S.; Yu, J. *J. Mater. Chem. B* **2018**, *6*, 5795−5801.
(40) Chen, J.; Luo, Z.; Sun, C.; Huang, Z.; Zhou, C.; Yin, S.; Duan, Y.; Li, Y. *Trends Anal. Chem.* **2019**, *120*, No. 115626.
(41) Liu, X.; Jiang, H.; Fang, Y.; Zhao, W.; Wang, N.; Zang, G. *Anal. Chem.* **2015**, *87*, 9163−9169.